Protein Science (1999), *8*:2338–2346. Cambridge University Press. Printed in the USA.

Mutations of endo-β-N-acetylglucosaminidase H active site residues Asp130 and Glu132: Activities and conformations

VIBHA RAO,[1] TAO CUI,[2] CHUDI GUAN,[2] AND PATRICK VAN ROEY[1]

[1]Division of Molecular Medicine, Wadsworth Center, New York State Department of Health, Albany, New York 12201-0509
[2]New England Biolabs Inc., Beverly, Massachusetts 01915

(RECEIVED June 8, 1999; ACCEPTED August 4, 1999)

Abstract

Endo-β-N-acetylglucosaminidase H hydrolyzes the β-(1–4)-glycosidic link of the *N,N′*-diacetylchitobiose core of high-mannose and hybrid asparagine-linked oligosaccharides. Seven mutants of the active site residues, Asp130 and Glu132, have been prepared, assayed, and crystallized. They include single site mutants of each residue to the corresponding amide, to Ala and to the alternate acidic residue, and to the double amide mutant. The mutants of Asp130 are more active than the corresponding Glu132 mutants, consistent with the assignment of the latter residue as the primary catalytic residue. The amide mutants are more active than the alternate acidic residue mutants, which in turn are more active than the Ala mutants. The structures of the Asn mutant of Asp130 and the double mutant are very similar to that of the wild-type enzyme. Several residues surrounding the mutated residues, including some that form part of the core of the β-barrel and especially Tyr168 and Tyr244, adopt a very different conformation in the structures of the other two mutants of Asp130 and in the Asp mutant of Glu132. The results show that the residues in the upper layers of the β-barrel can organize into two very distinct packing arrangements that depend on subtle electrostatic and steric differences and that greatly affect the geometry of the substrate-binding cleft. Consequently, the relative activities of several of the mutants are defined by structural changes, leading to impaired substrate binding, in addition to changes in functionality.

Keywords: β-barrel; endoglycosidase; glycohydrolase; site-directed mutagenesis

Endo-β-N-acetylglucosaminidase H (Endo H) is a 28.8 kDa glycohydrolase (Tarentino et al., 1974; Trimble & Maley, 1984), secreted by *Streptomyces plicatus* (Tarentino & Maley, 1974), that is widely used as a biochemical tool for the characterization and functional analysis of oligosaccharides and glycoproteins (Tarentino & Plummer, 1994; Maley et al., 1989; O'Neill, 1996). The enzyme hydrolyzes the central β-(1–4) bond of the *N,N′*-diacetylchitobiose core, GlcNAc-β(1–4)GlcNAc, of asparagine-linked oligosaccharides, leaving one N-acetylglucosamine (GlcNAc) attached to the protein while the other forms the reducing end of the released oligosaccharide. Endo H and three related endoglycosidases secreted by *Flavobacterium meningosepticum*, Endo F_1, Endo F_2, and Endo F_3 (Tarentino et al., 1992, 1993), are members of family 18 of the glycohydrolases (Henrissat, 1991; Davies & Henrissat, 1995; Henrissat & Davies, 1997). Other members of this family include chitinases from various origins. All enzymes of family 18 have similar $(\beta/\alpha)_8$-barrel folds in which the catalytic residues are located at the carboxyl end of β-strand 4 and act with retention of configuration. Unlike the chitinases, which all process chitin, a linear chain of β(1–4)-linked GlcNAc residues, the endoglycosidases process branched oligosaccharides and have specificities for distinct forms of asparagine-linked oligosaccharides. Endo H and Endo F_1 only process high-mannose oligosaccharides, requiring the following minimum substrate for activity: Manα(1–3)Manα(1–6)[Manα(1–3)]Manβ(1–4)GlcNAcβ(1–4)GlcNAc-Asn (Trimble & Maley, 1984). In contrast, Endo F_2 and Endo F_3 preferentially process biantennary and triantennary complex oligosaccharides (Tarentino & Plummer, 1994).

As part of our studies of the mechanism of action and the substrate specificities of these enzymes, the three-dimensional structures of Endo H and Endo F_1 were previously reported (Van Roey et al., 1994; Rao et al., 1995). The structures of the two enzymes are very similar and show the following characteristics: a β-hairpin in the loop of β-strand/loop/α-helix unit 2 that includes several highly conserved polar residues; absence of α-helices in units 5

Reprint requests to: Patrick Van Roey, Wadsworth Center, Empire State Plaza, P.O. Box 509, Albany, New York 12201-0509; e-mail: vanroey@wadsworth.org.

Abbreviations: Endo, endo-β-N-acetylglucosaminidase; FPLC, fast protein liquid chromatography; GlcNAc, N-acetylglucosamine; HEWL, hen egg white lysozyme; HPLC, high-performance liquid chromatography; Man, mannose; MBP, maltose binding protein; PEG, polyethylene glycol; WT, wild-type.

and 6; and, a shallow, curved cleft that runs from the loop 2 region to the area of units 5 and 6, across the carboxyterminal surface of the β-barrel. The loop 2 area was proposed to be the primary substrate recognition site, on the basis of the structural and functional similarity of this area in the two enzymes. This was further confirmed by the structure of hevamine, a family 18 chitinase, in complex with N,N',N''-triacetylchitotriose, in which the central GlcNAc was located in contact with a β-hairpin loop in unit 2 (Terwisscha van Scheltinga et al., 1994).

Schmidt and Lad (1994), on the basis of site-directed mutagenesis experiments in which every acidic residue of Endo H was converted to the corresponding amide, identified Asp130 and Glu132 as the putative catalytic residues. They proposed a catalytic mechanism, analogous to that of hen egg white lysozyme (HEWL), in which Glu132 would function as the general acid/proton donor and Asp130 as the oxocarbenium ion intermediate stabilizer/nucleophile. McCarter and Withers (1994) have determined that such a mechanism requires relative locations of the two acidic residues at average carboxylate oxygen separation distances of 5.3 and 9.5 Å, depending on whether the glycohydrolase functions by an inverting or retaining mechanism. However, the crystal structures of Endo H and Endo F_1 showed that Asp130 and Glu132 are in hydrogen-bonding contact with one another, at an average carboxylate oxygen separation distance of 4.2 for Endo H and 3.8 Å for Endo F_1. On the basis of the structure of hevamine in complex with allosamidin (Terwisscha van Scheltinga et al., 1995), a transition state analogue inhibitor of chitinases, it has been proposed that the family 18 glycohydrolases function via a substrate-assisted mechanism, involving only one acid residue (Terwisscha van Scheltinga et al., 1996; Tews et al., 1997). In this mechanism, Glu132 acts as the proton donor, and the N-acetyl group of the leaving GlcNAc acts as the nucleophile. Asp130 would stabilize the positive charge on the nitrogen of the N-acetyl group in the transition state intermediate. As part of our efforts at determining the respective role of the two residues, we prepared additional mutants of the two acidic residues and determined their crystal structures. The activities of the mutants are consistent with Glu132 playing the role of the acid in a substrate assisted hydrolysis mechanism but are affected in several cases by conformational changes in residues in the upper layers of the β-barrel that impair substrate binding.

Results

Relative enzymatic activities of Endo H mutants

Mutants of Endo H were prepared by site-directed mutagenesis and expressed using the pMAL fusion protein system (Riggs, 1994). Seven mutants of the two putative catalytic residues were prepared. Asp130 was replaced by Asn, Ala, and Glu, generating the D130N, D130A, and D130E variants, respectively. Similarly, Glu132 was replaced by Gln, Ala, and Asp, resulting in the mutants E132Q, E132A, and E132D, respectively. In addition, both acidic residues were replaced by their amide analogs in a double mutant D130N/E132Q. Table 1 lists the relative enzymatic activity of each of the mutants compared to that of the wild-type enzyme (WT). Gel shift assays, measuring the deglycosylation rate of RNase B under increasing concentrations of the enzyme, were performed with the purified fusion proteins prior to processing with Factor Xa. The HPLC assays for the fully processed and purified enzymes were performed according to published procedures, using dansylated Asn-$(GlcNAc)_2$-$(Man)_{5–8}$ as the substrate (Tarentino & Plummer, 1994). The activity levels obtained from both assays are very similar, confirming that the MBP component of the fusion protein does not affect the activity. The activity levels of the D130N and E132Q mutants are very similar to those reported by Schmidt and Lad (1994)—2 and 0.1%, respectively.

Table 1. *Relative activity of Endo H mutants at pH 5.5*

Mutant	RNase B gel shift % wt activity	HPLC assay % wt activity
D130N	1.25	3.14
D130E	0.1	0.21
D130A	0.1	0.04
E132Q	<0.05	0.05
E132D	0.05	0.03
E132A	Nondetectable	Nondetectable
D130N/E132Q	Nondetectable	Nondetectable

All mutants of Asp130 are more active than the corresponding Glu132 mutants. This confirms that the Glu plays a more important role in the mechanism of action than the Asp. D130N is much more active than all other mutants. The results of the HPLC assays, which are more accurate than the gel shift assays, suggest a slightly greater activity for the amide mutants compared to the alternate acidic residue mutants, which in turn appear to be more active than the Ala mutants. This is surprising because, on the basis of the chemical nature of the substitutions alone, the alternate acid residue mutants might have been expected to be more active than the amide and Ala mutants.

Our attempts to measure enzyme kinetic data for Endo H and related enzymes have failed, apparently due to product inhibition. Evidence for product inhibition has been obtained from competitive binding assays and by cocrystallization of Endo F_3 with oligosaccharides under conditions that include very low excess concentrations of the oligosaccharide (Waddling & Van Roey, unpubl. obs.). In the absence of enzyme kinetics results, which can separate enzymatic activity from substrate binding, determination of the three-dimensional structures was required to correlate these variations in activity with possible conformational effects of the mutations.

Crystallization and structure determination

The crystallization conditions and cell parameters are listed in Table 2. Only D130N crystallized under the same conditions and in the same space group and unit cell, as the WT enzyme. In this crystal form, Glu132 is involved in a crystal packing contact, consisting of a water-bridged contact with Glu135 of a symmetry-related molecule. Mutations of this residue destabilize this crystal packing, leading to inability to crystallize in this crystal form. Two of the Asp130 mutants, D130A and D130E, also did not crystallize in the WT form, despite a lack of changes in residues that are involved in intermolecular contacts. All crystallization solutions include polyethylene glycol (PEG) as the precipitant, but differ in the size and concentration of the PEG and in the presence or type of buffers and other additives. E132Q crystallized in space group P1 with two molecules in the asymmetric unit. In total, four different crystal forms have been obtained. The crystal structures of

Table 2. *Crystallization conditions for the seven mutants of Endo H*

Mutant	Crystal form	Unit cell	Drop[a]	Reservoir
D130N	Tetragonal I	$P4_32_12$ $a = b = 84.0$ Å $c = 88.2$ Å	4 μL protein 3 μL buffer 1 μL 20 mM OBG 4 μL water	100 mM cacodylate, pH 6.5 200 mM $Zn(Ac)_2$ 17% PEG8000
D130E	Monoclinic	$P2_1$ $a = 44.2$ Å, $b = 55.2$ Å $c = 46.2$ Å, $\beta = 103.8°$	2 μL protein 2 μL buffer	100 mM cacodylate, pH 6.1 30% PEG1000
D130A	Tetragonal II	$P4_32_12$ $a = b = 61.4$ Å $c = 140.9$ Å	2 μL protein + chitobiose (50×) 2 μL buffer	100 mM cacodylate, pH 6.5 100 mM $Zn(Ac)_2$ 25% PEG1000
E132Q	Triclinic	P1 $a = 47.9$ Å, $b = 54.3$ Å $c = 47.6$ Å $\alpha = 89.7°$, $\beta = 109.2°$ $\gamma = 84°$	4 μL protein 3 μL buffer 1 μL 20 mM OBG 4 μL water	100 mM cacodylate, pH 6.5 100 mM $Zn(Ac)_2$ 19% PEG1000
E132D	Tetragonal II	$P4_32_12$ $a = b = 61.4$ Å $c = 140.3$ Å	2 μL protein + chitobiose (50×) 2 μL buffer	100 mM cacodylate, pH 6.5 100 mM $Zn(Ac)_2$ 15% PEG1000
E132A	Monoclinic	$P2_1$ $a = 44.2$ Å, $b = 55.5$ Å $c = 46.8$ Å, $\beta = 104.1°$	3 μL protein 4 μL buffer	24% PEG1500
D130N/E132Q	Monoclinic	$P2_1$ $a = 44.3$ Å, $b = 55.5$ Å $c = 46.7$ Å, $\beta = 104.5°$	3 μL protein 6 μL buffer	34% PEG1500

[a]Buffer refers to the reservoir solution. Chitobiose (50×) refers to the addition of solid *N,N′*-diacetylchitobiose to the protein solution to a concentration that is approximately 50 times that of the protein.

the new tetragonal form and the monoclinic and triclinic forms were determined by molecular replacement methods. All structures were refined to 2.1 or 2.0 Å resolution. The data collection and refinement statistics are listed in Table 3.

Figure 1A shows the fold of Endo H, a $(\beta\alpha)_8$-barrel with the catalytic residue, Glu132, at the carboxy terminal end of β-strand 4. Figure 1B shows the superposition of the mutant structures onto the WT structure by least-squares fitting of the main-

Table 3. *Data collection and refinement statistics*

	D130N	D130E	D130A	E132Q	E132D	E132A	D130N/E132Q
Resolution Å	2.1	2.0	2.0	2.1	2.1	2.1	2.1
Completeness %	95.35	96.10	98.8	91.0	87.6	93.34	96.52
Completeness % (last shell)	74.4	92.7	96.2	88.0	83.0	90.2	92.3
Redundancy	6.60	3.09	3.11	3.00	1.89	3.84	3.15
R_{sym}	0.052	0.080	0.061	0.076	0.066	0.051	0.093
$\langle F^2/\sigma(F^2)\rangle$ last shell	3.22	2.38	4.29	5.64	7.09	3.57	4.48
R	0.218	0.197	0.209	0.212	0.215	0.218	0.205
Water molecules	255	152	288	319	203	156	125
B_{ave}							
Main chain (Å^2)	25.15	14.92	16.78	15.91	20.38	25.66	17.27
Side chain (Å^2)	27.07	16.23	18.23	17.16	22.19	26.70	18.31
Water (Å^2)	41.93	22.68	33.03	23.45	34.84	35.58	26.34
RMSD bond length (Å)	0.011	0.012	0.010	0.013	0.011	0.012	0.013
Bond angle (deg)	1.613	1.725	1.586	1.655	1.609	1.682	1.685
Dihedral (deg)	25.14	25.42	24.88	25.18	24.98	25.69	25.73
Impropers (deg)	1.41	1.58	1.41	1.51	1.36	1.52	1.46

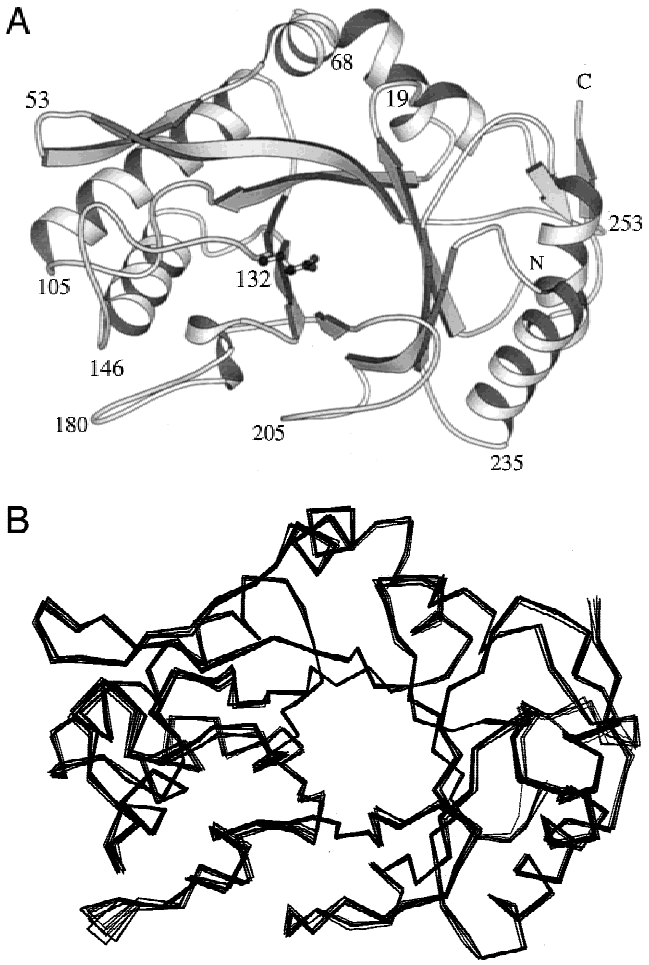

Fig. 1. A: Ribbon diagram of the structure of Endo H with the catalytic residue Glu132 shown. The location of the amino- and carboxy-termini and several residues on loops are shown to assist in orientation. **B:** Superposition of the α-carbon tracings of the nine molecules of Endo H and its mutants. Figures 1, 2, and 3 were prepared with MOLSCRIPT, version 2.1.2. (Kraulis, 1991).

chain atoms. The fit results in root-mean-square deviations (RMSDs) in the range of 0.34 to 0.62 Å, with the smallest ones observed for D130N and E132Q and the largest one for D130E. As anticipated, all the larger differences between the structures are found in the amino- and carboxy-termini and in loops on the surface of the molecules and result from differences in the crystal packing.

Two loops adjacent to the substrate-binding cleft, those following β-strands 3 and 4, undergo significant changes in conformation as a result of differences in the crystal packing. In the WT form, these loops are involved in intermolecular interactions. The most specific contacts are a salt bridge between His94 (loop 3) and Glu217 of a symmetry-related molecule and an indirect contact, bridged by a water molecule or a metal ion, between the catalytic residue Glu132 (loop 4) and Glu135 of a symmetry-related molecule. In the other crystal forms, intermolecular contacts in this area are limited to weak, less specific contacts of loop 3 residues in the monoclinic and triclinic forms. Main-chain atoms of residues 92 to 98 and 132 to 143 are displaced by up to 2 Å. Most noteworthy are the 180° flips of the peptide links between Ser93 and His94 and between Glu132 and Tyr133. The change in the conformation of loop 4 does not significantly alter the position of the side chain of Glu132 relative to other active site residues but is correlated with a smaller and a larger change in the side-chain conformations of Tyr133 and His94, respectively. Because these two residues are at the edge of the substrate binding cleft, the flexibility of the loops may be of importance for substrate binding.

Active site conformation

Figure 2 compares the conformations of all residues in the active site area, including the mutated residues, the upper layer of the β-barrel, and the surrounding residues that form the walls of the cleft above the barrel. The side-chain dihedral angles of the residues that show the largest variation in their conformation are listed in Table 4. The geometry of residue 130, which is confined within the upper level of the barrel, is not affected by mutation to Asn or by any mutation of residue 132. The carboxylate group of Glu130, in D130E, extends slightly above the upper layer of the barrel and swings away from Glu132 to form a hydrogen bond with Oγ of Ser89. Residue 132, as a Glu or Gln, adopts two distinct conformations. The conformation seen in the WT enzyme and mutants D130N, E132Q, and D130N/E132Q allows a weak hydrogen bonding interaction with the side chain of 130, with a distance of 2.9 to 3.4 Å. In the mutants D130A and D130E, the Glu132 side chain lacks its hydrogen-bonding partner and is rotated away. As an Asp, in E132D, residue 132 also rotates away from Asp130.

Asp130 and Glu132 are surrounded in the substrate binding cleft by several aromatic residues, Tyr14, Phe44, Tyr133, Tyr168, Tyr196, and Tyr244. The side chains of several of these residues adopt different conformations in the structures of the mutants, resulting in two distinct active site geometries. In the first, which is seen in the WT structure and mutants D130N, E132A, and D130N/E132Q, the plane of the phenyl ring of Tyr168 is parallel to the plane of the barrel and that of Tyr244 is perpendicular, with its hydroxyl group pointing upward. In the second geometry, seen in D130E, D130A, and E132D, Tyr244 is parallel to the barrel surface while Tyr168 is perpendicular, and it hydroxyl group points upward out of the cleft. The two remaining molecules, the two independent observations of E132Q, adopt a conformation that is intermediate between the two groups. Both molecules have Tyr244 in the WT conformation. The plane of the phenyl ring of Tyr168 is perpendicular to the barrel plane in both molecules, as in the structures of the second class, but its hydroxyl group points into the cleft in molecule E132Qa and out of the cleft in molecule E132Qb.

Two other residues that are part of the binding cleft, Glu16 and Leu91, adopt different conformations in the nine molecules. However, the variation in the conformations of these two residues cannot be correlated directly with electrostatic or steric hindrance effects of the mutations. These residues are located in a more exposed area of the substrate binding cleft. Consequently, their conformations are determined by a combination of effects related to the mutations and to crystal packing effects, such as the change in the loop 3 conformation.

Discussion

Barrel packing

The $(\beta/\alpha)_8$-barrel proteins represent one of the most commonly observed folds, and the geometry of the β-barrel has been re-

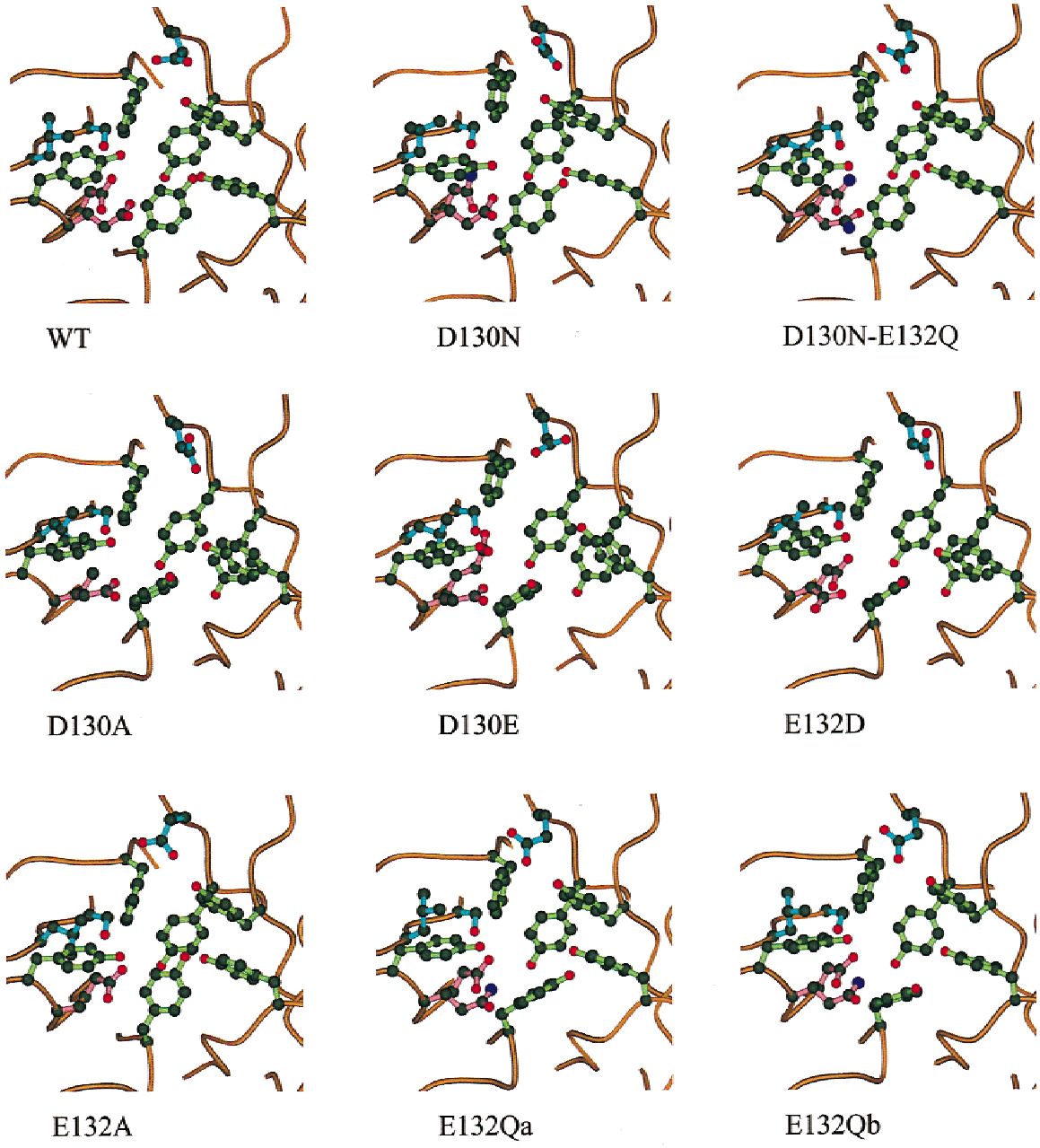

Fig. 2. Conformations of the active site residues and the top layer of the barrel in the nine molecules of Endo H and the mutants. The mutated residues 130 and 132 are colored pink. The aromatic residues surrounding the active site are colored green. Three additional residues in the substrate binding cleft are colored blue. Residues, in clockwise order from the top center of the figure, are: Glu17, Tyr14, Tyr244, Tyr196, Tyr168, Slu132, Asp130, Tyr133, Leu91, Ser89, and Phe44.

viewed extensively (Farber & Petsko, 1990; Lesk et al., 1989; Raine et al., 1994; Sergeev & Lee, 1994). The barrel is composed of eight parallel β-strands connected by a tight hydrogen-bonding network. Every other residue on a strand extends its side chain into the core of the barrel. These core residues tend to be large, hydrophobic residues and are arranged in layers, with each layer containing four residues from alternating β-strands. At least three layers are ordered in a sufficiently regular manner to define the core of the barrel. Additional residues at either end of the β-strands frequently extend the height of the barrel but are not necessarily arranged in a regular pattern or include smaller residues that reduce the packing density.

Endo H has four layers of regularly packed side chains and two additional irregular layers, one below and one above the barrel, as shown in Table 5. Pro194 and Pro213 introduce kinks in β-strands 6 and 7, respectively, disrupting the regular alternating residue pattern of these strands, but not the packing. Residue 130 is located in the upper barrel layer, and its carboxylate group forms part of the bottom of the substrate binding cleft. It is therefore not surprising that mutations that affect the size of this residue allow

Table 4. *Side-chain conformations of residues in the substrate binding cleft and upper layer of the β-barrel*

Residue	WT	D130N	D130A	D130E	E132Qa	E132Qb	E132A	E132D	D130N/E132Q
Asp130									
$\chi 1$	−172.8	−169.5	—	−69.6	−171.0	−174.2	−167.2	178.9	−173.9
$\chi 2$	−5.3	19.6	—	−177.1	−10.5	−21.4	−13.6	−7.9	−3.8
Glu132									
$\chi 1$	−115.0	−95.5	−166.3	−165.4	−67.8	−80.2	—	−137.4	−55.7
$\chi 2$	−163.0	−163.3	172.2	170.5	−174.2	−169.1	—	169.0	−159.3
$\chi 3$	110.3	−64.6	−163.5	−166.4	93.5	108.7	—	—	−104.9
Phe14									
$\chi 1$	−86.8	−83.1	−92.8	−90.9	−86.1	−90.5	−88.2	−90.9	−86.9
$\chi 2$	−114.5	−109.4	−120.9	−111.2	−113.6	−70.4	−111.3	−123.2	−122.4
Tyr44									
$\chi 1$	−165.1	179.3	−165.5	178.0	−172.1	−174.1	−158.0	−163.8	−166.9
$\chi 2$	78.5	91.7	80.9	88.8	95.1	84.5	70.7	77.6	97.7
Tyr133									
$\chi 1$	−37.1	−49.4	−49.7	−46.2	−55.0	−52.4	−44.8	−47.2	−41.0
$\chi 2$	133.7	129.9	121.6	124.9	126.2	117.9	130.2	130.8	140.1
Tyr168									
$\chi 1$	−101.5	−125.3	177.8	172.5	−136.3	175.1	−90.9	171.6	−98.0
$\chi 2$	−69.7	−58.0	76.6	87.0	−120.8	77.2	−80.9	−94.2	−89.0
Tyr196									
$\chi 1$	−50.6	−52.7	−38.6	−40.3	−53.3	−52.9	−48.4	−39.9	−52.8
$\chi 2$	106.2	115.0	−27.2	158.1	119.8	106.7	125.6	−30.5	130.0
Tyr244									
$\chi 1$	171.2	172.8	−67.6	−67.5	164.5	152.3	162.8	−69.2	167.2
$\chi 2$	73.8	81.6	96.5	97.1	87.6	91.5	81.6	94.5	85.0
Glu16									
$\chi 1$	−59.0	−66.9	−67.1	−63.5	−76.7	−75.4	−157.9	−67.2	−62.4
$\chi 2$	−140.5	−168.3	173.4	−175.5	−87.9	−98.5	70.7	162.0	−118.9
$\chi 3$	−117.7	31.3	9.3	−75.1	175.8	172.0	57.5	6.5	20.1
Leu91									
$\chi 1$	76.0	56.0	−173.6	−113.6	80.2	80.2	−122.8	178.3	−105.3
$\chi 2$	176.4	100.8	72.5	−170.5	162.5	167.2	−168.8	76.0	174.4

packing of this layer in a different conformation. Interestingly, lengthening and shortening the side chain of residue 130 have identical effects. Although Glu is a larger residue than Asp, it is less bulky around Cγ, which is at the level where the packing in the upper layer of the barrel is most dense. Consequently, this substitution reduces the steric constraints within the layer in a similar fashion as the Asp to Ala mutation, resulting in similar packing. Glu130 does form an additional hydrogen-bonding con-

Table 5. *Residues in the core layers of the β-barrel of Endo H*[a]

	Strand							
Layer	1	2	3	4	5	6	7	8
5	Glu16		Leu91				Glu217	
4		Phe44		Asp130		Tyr196		Tyr244
3	Tyr14		Ser89		Tyr168		Ala215	
2		Val42		Asp128		Trp192		Leu242
1	Val12		Leu87		Ser166		Ser212	
0		Val40		Gly126		Tyr190		Val240

[a]Layers 1–4 are have regular packing, while layers 0 and 5 are more irregular or incomplete.

tact with Ser89; however, this contact is made above the upper layer of the barrel. It is more difficult to explain why a Glu to Asp mutation at residue 132 would have a similar effect on the barrel packing as the changes in the size of residue 130. Glu132 is the first residue of loop 4 and extends into the binding cleft from the side wall. It does not interact with any residue in the upper layer of the barrel, other than the weak hydrogen bond with Asp130 in the WT enzyme or with Asn130 in D130N.

The residues that undergo major changes in conformation include one residue from the second layer, Tyr168. The remaining residues in the lower layers of the barrel are unchanged, except for Trp192, which is one layer below but close to Tyr168 and which differs by rotation of about 10° between the two packing arrangements.

These results suggest that a slight reduction in the packing density in the upper layer of the β-barrel of Endo H allows the residues in this layer to pack in a different manner, largely independent from changes in the conformations of the residues in the other layers. Both packing arrangements are probably very similar in energy, in view of the fact that the E132D mutant has the conformation of the D130A and D130E mutants and that Tyr168, but not Tyr244, is observed in the mutant conformation in E132Q. In addition, no evidence of cavities, strain in the main-chain conformation, or loss of hydrogen bonding contacts is observed. Tyr168 and Tyr196, although very different in conformation, are in hydrogen bonding contact in both packing arrangements.

Comparison with the packing of the equivalent residues in Endo F_1 (Van Roey et al., 1994), the closest analog to Endo H, shows that Tyr171 and Tyr199, the equivalents of Tyr168 and Tyr196, respectively, are not exactly in the same location. Both residues are displaced by about 1.00 Å, with Tyr171 closer to the conformation observed for Tyr168 in D130E than to the WT conformation. On the other hand, Phe249, the equivalent of Tyr244 is in the WT conformation. This, together with the conformations of Tyr168 observed in the E132Q mutant structures, suggests that Tyr168 is indeed more flexible, and it is possible that the alternate conformation of this residue is the one most suitable for substrate binding.

Despite the flexibility of Tyr168, it is very unlikely that the folded protein can exchange between the two conformations observed for the other residues. Transformations in the conformations of Tyr196 and Tyr244 require movement by several other residues, especially, Tyr44, Glu16, and Glu217. Therefore, the observed conformations are most likely defined during protein folding.

Structure–activity correlation

The rearrangement of the residues in the base of the substrate binding cleft greatly alters the surface geometry within the cleft and changes the position and orientation of tyrosine rings and their hydroxyl groups, which are contact points for substrate binding through hydrophobic interactions and hydrogen bonding, respectively. The differences in the geometry of the binding clefts of the WT enzyme and the D130E mutant are shown in Figure 3. The cleft in the WT conformation is deeper in the areas of residues Phe44 and Tyr168. In the conformation of D130E, the hydroxyl group of Tyr244 is unavailable for hydrogen bonding with the substrate, while that of Tyr196 is displaced by more than 1.0 Å. Therefore, it is unlikely that the substrate can bind efficiently in the binding cleft of the mutants with alternate packing arrangement.

The variation in the activities of the three mutants of Asp130 can be correlated with the effects of the mutations on the conformation of the surrounding residues. D130N has the highest activity of all mutants. This mutation does not affect the protein conformation, maintains a polar residue at this position but removes the negative charge. The activity of this mutant is significantly higher than that of the Asn mutant of HEWL Asp52 (Matsumura & Kirsch, 1996), the nucleophile/oxocarbenium-stabilizing residue. This high activity of D130N indicates that Asp130 of Endo H plays a lesser role than Asp52 of HEWL. This evidence, combined with the similarity of the Endo H active site to that of hevamine rather than to that of HEWL, suggest that Endo H functions by the substrate assisted hydrolysis mechanism. In this mechanism, Asp130 does not take a direct role in the mechanism, but stabilizes the intermediate through interaction with a positively charge nitrogen. Ac-

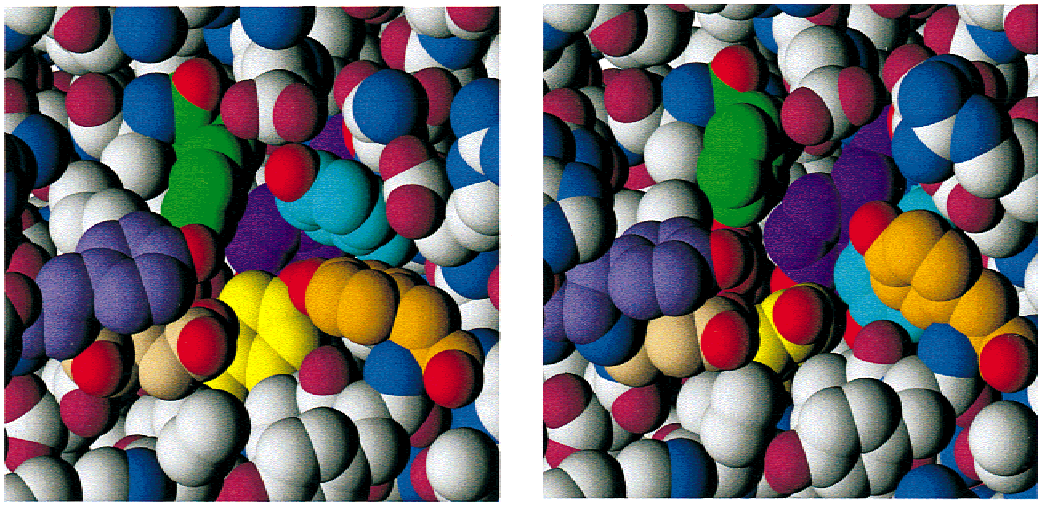

Fig. 3. Space-filling model of the active site area of Endo H in the WT form and in the D130E mutant. Residue colors: Phe44, green; Tyr14, purple; Tyr244, light blue; Tyr196, orange; Tyr168, yellow; Glu132, beige; Tyr133, violet.

tivity levels of D130E and D130A are affected by the conformational changes that interfere with substrate binding and likely lower than they would be in absence of this conformational change.

Likewise, the low activity of the E132D mutant is, in part, caused by the altered substrate-binding surface, while inactivity of the E132A mutant is a purely catalytic effect. Although Tyr168 adopts two non-WT conformations in the two structures of the E132Q mutant, all other residues in the substrate binding cleft are in the WT conformation, suggesting that this conformation is equally accessible, and the low activity is consistent with catalytic effects only. The low but measurable activity of E132Q is, considering the inability of a Gln, to function, as the acid in the mechanism is somewhat surprising, but may be a result of spontaneous deamination.

Materials and methods

Mutagenesis, expression, and purification

Site-directed mutagenesis was carried out using the Kunkel method (Kunkel et al., 1991). The DNA encoding for Endo H was cloned into the *Bam*H I and *Hin*d III site of PMAL-p2 plasmid. The required mutation in the Endo H gene was introduced by site-directed mutagenesis using 39 base-pair synthesized oligonucleotides with the site of mutation at positions 19 to 21 for the Asp130 mutants and 25 to 27 for the Glu132 mutants. All mutations were confirmed by DNA sequencing. Expression of the gene products was carried out using the method described by Riggs (1994). The fusion proteins were purified over an amylose column and digested with 1% factor Xa overnight. The Endo H mutant proteins were separated from MBP and Factor Xa by FPLC on a Mono Q column.

Enzymatic activity of the MBP-Endo H mutant fusion proteins was determined by enzyme–concentration-dependent gel-shift assays of the deglycosylation of denatured RNase B. The activities of the fully processed and purified mutant proteins were compared to that of the wild-type (WT) enzyme by an HPLC assay with dansylated Asn-$(GlcNAc)_2$-$(Man)_{5–8}$ as the substrate (Tarentino & Plummer, 1994).

Crystallization

Crystals were grown by hanging-drop, vapor-diffusion methods at room temperature. Initially, crystallization experiments for all the mutants were set up under conditions similar to those used for the WT enzyme, but only the D130N mutant crystallized under these conditions. Sparse matrix sampling methods (Jancarik & Kim, 1991), with Crystal Screen Kit I (Hampton Research, Laguna Niguel, California), were used to identify initial conditions for crystallization of the remaining mutants. The precipitation buffers used for the mutants D130A, E132Q, and E132D are related to the WT conditions but with a lower zinc acetate concentration and PEG1000 in place of PEG8000. All other crystallization conditions included PEG as the primary precipitating agent. In several cases, addition of low concentration n-octyl-β-D-glucopyranoside or high concentrations of *N,N′*-diacetylchitobiose was beneficial to the growth of larger single crystals.

X-ray diffraction

All X-ray diffraction data were measured on a Rigaku R-axis IIc image plate area detector with CuKα radiation generated by a Rigaku RU-200 rotating anode source equipped with MSC/Yale mirror optics. All the crystals were flashcooled in the cold nitrogen gas stream of a liquid nitrogen low-temperature device (MSC) to approximately $-150\,^{\circ}C$ immediately after addition of 5 to 10 μL of cryoprotectant to the crystallization drop. Twenty percent glycerol or 30% PEG1500 was used as the cryoprotectant for the D130N, E132A, E132Q, and D130N/E132Q mutants, and the crystallization buffer supplemented with 20% PEG1000 was used for the D130A and E132D mutants. No additional cryoprotectant was used for the D130E mutant because the crystallization buffer already contained 30% PEG1000. All the crystals diffracted to 2.0 or 2.1 Å. The monoclinic and triclinic crystals are much thinner than the tetragonal crystals but due to the smaller unit cell and the higher density diffract equally well.

Structure determination

The refined WT structure was used as the starting model for the refinement of D130N. All refinements were started by a cycle of rigid body refinement followed by simulated annealing (Brünger et al., 1987; Brünger, 1988). The structures of E132A (monoclinic), D130A (tetragonal II), and E132Q (triclinic) were determined by molecular replacement methods, using the WT structure as the model. The molecular replacement routines of X-PLOR, version 3.1 (Brünger, 1990), were used to determine the structure of E132A, while AMORE (Navaza, 1994), as implemented in the CCP4 package, version 2.15 (CCP4, 1994), was used to determine the structures of D130A and E132Q. After partial refinement, the D130A and E132A structures were used as the starting models for the other mutants that crystallized in the corresponding crystal forms. All structures were refined by simulated annealing, as implemented in X-PLOR 3.1. After the initial slow-cooling protocol including data to 2.8 Å, further refinement was carried out using alternating cycles of standard positional and individual restrained temperature factor refinement as well as model building using CHAIN (Sack, 1988). Sites of mutation were examined using omit maps, for which all residues within a sphere of 8 Å radius around the mutated residue were removed and the rest of the model subjected to refinement. The stereochemical parameters of the models were evaluated with the geometry analysis features of X-PLOR and the program PROCHECK (Laskowski et al., 1993). The final models of all the structures contain 265 of the 271 residues. Electron density could not be seen for five amino-terminal residues and for one carboxy-terminal residue in all structures. Ala45 is in a *cis* conformation in all structures. No nonglycine residues fall outside the "additionally allowed" region of the Ramachandran plots. Atomic coordinates have been deposited with the Protein Data Bank under accession codes 1C3F (D130N), 1C8X (D130E), 1C8Y (D130A), 1C90 (E132Q), 1C91 (E132D), 1C92 (E132A), and 1C93 (D130N/E132Q).

Acknowledgments

We thank T.H. Plummer, Jr., for performing the HPLC assays. Research supported by grant GM-50431 from the National Institute of General Medical Sciences, National Institutes of Health.

References

Brünger AT. 1988. Crystallographic refinement by simulated annealing. Application to a 2.8 Å resolution structure of aspartate aminotransferase. *J Mol Biol 203*:803–816.

Brünger AT. 1990. Extension of molecular replacement: A new search strategy based on Patterson correlation refinement. *Acta Crystallogr A46*: 46–57.

Brünger AT, Kuriyan J, Karplus M. 1987. Crystallographic *R*-factor refinement by molecular dynamics. *Science 235*:458–460.

CCP4 (Collaborative Computing Project Number 4). 1994. Collaborative computing project No. 4. The CCP4 suite: Programs for protein crystallography. *Acta Crystallogr D50*:760–763.

Davies G, Henrissat B. 1995. Structures and mechanisms of glycosyl hydrolases. *Structure 3*:853–859.

Farber GK, Petsko GA. 1990. The evolution of alpha/beta barrel enzymes. *Trends Biochem Sci 15*:228–234.

Henrissat B. 1991. A classification of glycosyl hydrolases based on amino acid sequences. *Biochem J 280*:309–316.

Henrissat B, Davies G. 1997. Structural and sequence-based classification of glycoside hydrolases. *Curr Opin Struct Biol 7*:637–644.

Jancarik J, Kim SH. 1991. Sparse matrix sampling: A screening method for crystallization of proteins. *J Appl Crystallogr 24*:409–411.

Kraulis PJ. 1991. MOLSCRIPT: A program to produce both detailed and schematic plots of protein structures. *J Appl Crystallogr 24*:946–950.

Kunkel TA, Bebenek K, McClary J. 1991. Efficient site-directed mutagenesis using uracil-containing DNA. *Methods Enzymol 204*:125–139.

Laskowski RA, McArthur MW, Moss DS, Thornton JM. 1993. PROCHECK: A program to check the stereochemical quality of protein structures. *J Appl Crystallogr 26*:282–291.

Lesk AM, Branden CI, Chothia C. 1989. Structural principles of alpha/beta barrel proteins: The packing of the interior of the sheet. *Proteins Struct Funct Gen 5*:139–148.

Maley F, Trimble RB, Tarentino AL, Plummer TH Jr. 1989. Characterization of glycoproteins and their associated oligosaccharides through the use of endoglycosidases. *Anal Biochem 180*:195–204.

Matsumura I, Kirsch JF. 1996. Is aspartate 52 essential for catalysis by chicken egg white lysozyme? The role of natural substrate-assisted hydrolysis. *Biochemistry 35*:1881–1889.

McCarter JD, Withers SG. 1994. Mechanisms of enzymatic glycoside hydrolysis. *Curr Opin Struct Biol 4*:885–892.

Navaza J. 1994. AmoRe: An automated package for molecular replacement. *Acta Crystallogr A50*:157–163.

O'Neill RA. 1996. Enzymatic release of oligosaccharides from glycoproteins for chromatographic and electrophoretic analysis. *J Chromatogr A 720*:201–215.

Raine ARC, Scrutton NS, Mathews FS. 1994. On the evolution of alternate core packing in eightfold β/α-barrels. *Protein Sci 3*:1889–1892.

Rao V, Guan C, Van Roey P. 1995. Crystal structure of endo-β-N-acetylglucosaminidase H at 1.9 Å resolution: Active-site geometry and substrate recognition. *Structure 3*:449–457.

Riggs P. 1994. Expression and purification of maltose binding protein fusions. *Curr Protein Mol Biol 2*:16.6.1–16.6.10.

Sack JS. 1988. CHAIN—A crystallographic modeling program. *J Mol Graph 6*:244–245.

Schmidt BF, Lad P. 1994. Identification of two aspartates and a glutamate essential for activity of endo-β-N-acetylglucosaminidase H from *Streptomyces plicatus*. *Arch Biochem Biophys 311*:350–353.

Sergeev Y, Lee B. 1994. Alignment of β-barrels in $(\beta/\alpha)_8$ proteins using hydrogen-bonding pattern. *J Mol Biol 244*:168–182.

Tarentino AL, Maley F. 1974. Purification and properties of an endo-β-N-acetylglucosaminidase from *Streptomyces griseus*. *J Biol Chem 249*:811-817.

Tarentino AL, Plummer TH Jr. 1994. Enzymatic deglycosylation of asparagine-linked glycans: Purification, properties, and specificity of oligosaccharide-cleaving enzymes from *Flavobacterium meningosepticum*. *Methods Enzymol 230*:44–57.

Tarentino AL, Plummer TH Jr, Maley F. 1974. The release of intact oligosaccharides from specific glycoproteins by endo-β-N-acetylglucosaminidase H. *J Biol Chem 249*:818–824.

Tarentino AL, Quinones G, Changchien LM, Plummer TH Jr. 1993. Multiple endoglycosidase F activities expressed by *Flavobacterium meningosepticum* endoglycosidases F_2 and F_3. Molecular cloning, primary sequence, and enzyme expression. *J Biol Chem 268*:9702–9708.

Tarentino AL, Quinones G, Schrader WP, Changchien LM, Plummer TH Jr. 1992. Multiple endoglycosidase (Endo) F activities expressed by *Flavobacterium meningosepticum*. Endo F_1: Molecular cloning, primary sequence, and structural relationship to Endo H. *J Biol Chem 267*:3868–3872.

Terwisscha van Scheltinga AC, Armand S, Kalk KH, Isogai A, Henrissat B, Dijkstra BW. 1995. Stereochemistry of chitin hydrolysis by a plant chitinase/lysozyme and X-ray structure of a complex with allosamidin: evidence for substrate assisted catalysis. *Biochemistry 34*:15619–15623.

Terwisscha van Scheltinga AC, Hennig M, Dijkstra BW. 1996. The 1.8 Å resolution structure of hevamine, a plant chitinase/lysozyme, and analysis of the conserved sequence and structure motifs of glycosyl hydrolase family 18. *J Mol Biol 262*:243–257.

Terwisscha van Scheltinga AC, Kalk KH, Beintema JJ, Dijkstra BW. 1994. Crystals structures of hevamine, a plant defence protein with chitinase and lysozyme activity, and its complex with an inhibitor. *Structure 2*:1181–1189.

Tews I, Terwisscha van Scheltinga AC, Perrakis A, Wilson KS, Dijkstra BW. 1997. Substrate-assisted catalysis unifies two families of chitinolytic enzymes. *J Am Chem Soc 119*:7954–7959.

Trimble RB, Maley F. 1984. Optimizing hydrolysis of N-linked high-mannose oligosaccharides by endo-β-N-acetylglucosaminidase H. *Anal Biochem 141*:515–522.

Van Roey P, Rao V, Plummer TH Jr, Tarentino AL. 1994. Crystal structure of endo-β-N-acetylglucosaminidase F_1, an α/β-barrel enzyme adapted for a complex substrate. *Biochemistry 33*:13989–13996.